REVIEW ARTICLE

Liquid Phase Transmission Electron Microscopy for Nanomaterial Dynamics and Applications

Ziming Shang[1,†], **Yu Su**[1,†], **Yi Chen**[2] **and Qiubo Zhang**[1,*]

[1] SEU-FEI Nano-Pico Center, Key Lab of MEMS of Ministry of Education, School of Integrated Circuits, Southeast University, Nanjing 210096, China
[2] Materials Sciences Division, Lawrence Berkeley National Laboratory, Berkeley 94720, United States

Abstract

Nanomaterials play crucial roles in energy, catalysis, biomedicine, and electronic devices. A systematic and in-depth understanding of the dynamic behavior during structural evolution and practical applications is significant. Liquid phase transmission electron microscopy (LP-TEM) is a powerful in situ characterization technique. It provides atomic-scale resolution and high temporal resolution observation for the evolution of nanomaterials in solution and has become a crucial tool for studying the dynamic processes of nanomaterials. This review summarizes the latest research progress of LP-TEM in nanomaterial nucleation and growth, etching and corrosion, self-assembly, and electrochemical applications, which is significant for understanding the developmental trajectory of liquid phase electron microscopy. Furthermore, this review outlines the challenges currently faced by LP-TEM and provides perspectives on future strategies to overcome these limitations. This review aims to provide a new perspective for broader nanomaterials research and to expand the application of LP-TEM in nanomaterials research.

Keywords: liquid phase TEM, nanomaterials, nucleation and growth, etching and corrosion, assembly, electrochemistry.

1 Introduction

Nanomaterials have unique physicochemical properties, such as surface effects, quantum effects, and size effects, and play critical roles in catalysis, clean energy production [1], biomedicine [2], and microelectronic devices [3]. Dynamic morphological evolution of nanomaterials during synthesis and application directly influences their properties. Therefore, a systematic and in-depth understanding of these dynamic processes is essential. Conventional ex situ characterization techniques, such as X-ray diffraction (XRD), Fourier-transform infrared spectroscopy (FTIR), and ex situ transmission electron microscopy (TEM), only provide post-reaction analysis and lack the capability for real-time observation. Moreover, dynamic processes including nanoparticle nucleation and growth, etching and

Submitted: 31 March 2026
Accepted: 13 May 2026
Published: 28 May 2026

Vol. 2, **No.** 2, 2026.
10.62762/JAMR.2026.738602

***Corresponding author:**
✉ Qiubo Zhang
qiubozhang@seu.edu.cn

† These authors contributed equally to this work

Citation
Shang, Z., Su, Y., Chen, Y., & Zhang, Q. (2026). Liquid Phase Transmission Electron Microscopy for Nanomaterial Dynamics and Applications. *Journal of Advanced Materials Research*, 2(2), 151–168.

corrosion, self-assembly, and dendrite growth in lithium batteries often take place in liquid environments or at solid–liquid interfaces. However, traditional transmission electron microscopy requires a high-vacuum sample chamber, making it difficult for liquid samples to remain stable. Therefore, an in situ characterization technique capable of directly capturing the real-time evolution of nanomaterials in liquid phase environments is needed to bridge the existing gap in understanding.

LP-TEM provides a method for imaging dynamic processes in liquid environments with atomic-scale spatial resolution and high temporal resolution. LP-TEM seals a thin liquid layer within the closed window (Liquid Cell), thereby isolating it from the vacuum environment to achieve compatibility with liquid samples. As a result, LP-TEM has become a revolutionary tool for bridging the research gap of visualizing the dynamics of materials in solution. Incidentally, silicon nitride (SiN_x) liquid cells [46] and graphene liquid cells [5] are common liquid cell types. In recent years, LP-TEM has achieved significant progress in revealing the mechanisms of morphological evolution in nanomaterials, fundamentally reshaping the understanding of dynamic processes such as nucleation and growth of nanomaterials and interfacial evolution. Thereby, LP-TEM overcomes the limitations of conventional theories and previous characterization techniques.

This review summarizes early landmark studies and recent developments in LP-TEM studies of nanomaterial dynamics. We first discuss the recent progress of LP-TEM studies in nanomaterial nucleation and growth, etching and corrosion, and self-assembly, including nonclassical growth pathways, etching and corrosion under complex controlling factors, and intricate self-assembly of nanomaterials from 1D to 3D architectures. We then provide a comprehensive overview of LP-TEM applications in the field of nano electrochemistry, especially battery interfaces and electrocatalytic reactions. Finally, we highlight the current limitations and challenges faced by LP-TEM research and provide perspectives on future directions for its future development.

2 LP-TEM Studies for Nanomaterial Dynamics

2.1 Nucleation and Growth

During nanomaterial synthesis, the nucleation and growth processes influence the shape and structure of nanomaterials, then determining their physicochemical characteristics. Therefore, it is important to investigate the growth dynamics of nanomaterials. Classical theories often illustrate the influence of thermodynamic factors such as surface free energy during nucleation and growth. The LaMer model [6] and the Ostwald ripening model [7] describe nanoparticle nucleation and maturation from a thermodynamic perspective. The LaMer model provides a classical description of nucleation and growth of nanoparticles in solution, rapid nucleation occurs when the precursor concentration reaches a critical supersaturation level, leading to extensive consumption of the precursor, followed by continued growth of the nuclei through diffusion after nucleation ceases. The Ostwald ripening model describes the growth tendency of differently sized particles in solution: smaller particles with higher surface energy tend to dissolve, while larger particles are thermodynamically stable due to their lower surface energy and grow by redeposition of dissolved species.

However, beyond thermodynamics, kinetic factors such as interparticle interactions and ligand migration can influence the growth process of nanomaterials and lead to non-classical growth pathways. Studies on these non-classical nucleation and growth mechanisms are essential to understanding the decisive factors during the early stages of material formation. LP-TEM provides real-time, high-resolution visualization of dynamic processes in liquid environments, making it a powerful tool for tracking the growth trajectories of nanomaterials. As early as 2009, Zheng *et al.* [4] employed LP-TEM to observe the nucleation and growth of Pt nanocrystals with sub-nanometer resolution. In addition to classical monomer attachment, the study revealed that particle coalescence is another pathway of growth. Furthermore, they discovered that structural relaxation occurs after particle coalescence, growth of the particles ceases at this stage, leading to a narrow size distribution of nanoparticles. Figure 1(a) shows the two growth pathways. This study not only applied LP-TEM to visualizing nanocrystal growth in solution for the first time, but also revealed a new pathway for nanomaterials growth, leading to revisions of traditional nucleation and growth theories.

In addition to coalescence, oriented attachment—a process involving the fusion of nanocrystals following crystallographic coalignment—is another common pathway in nanomaterial growth. Li *et al.* [8] employed LP-TEM with lattice resolution to visualize

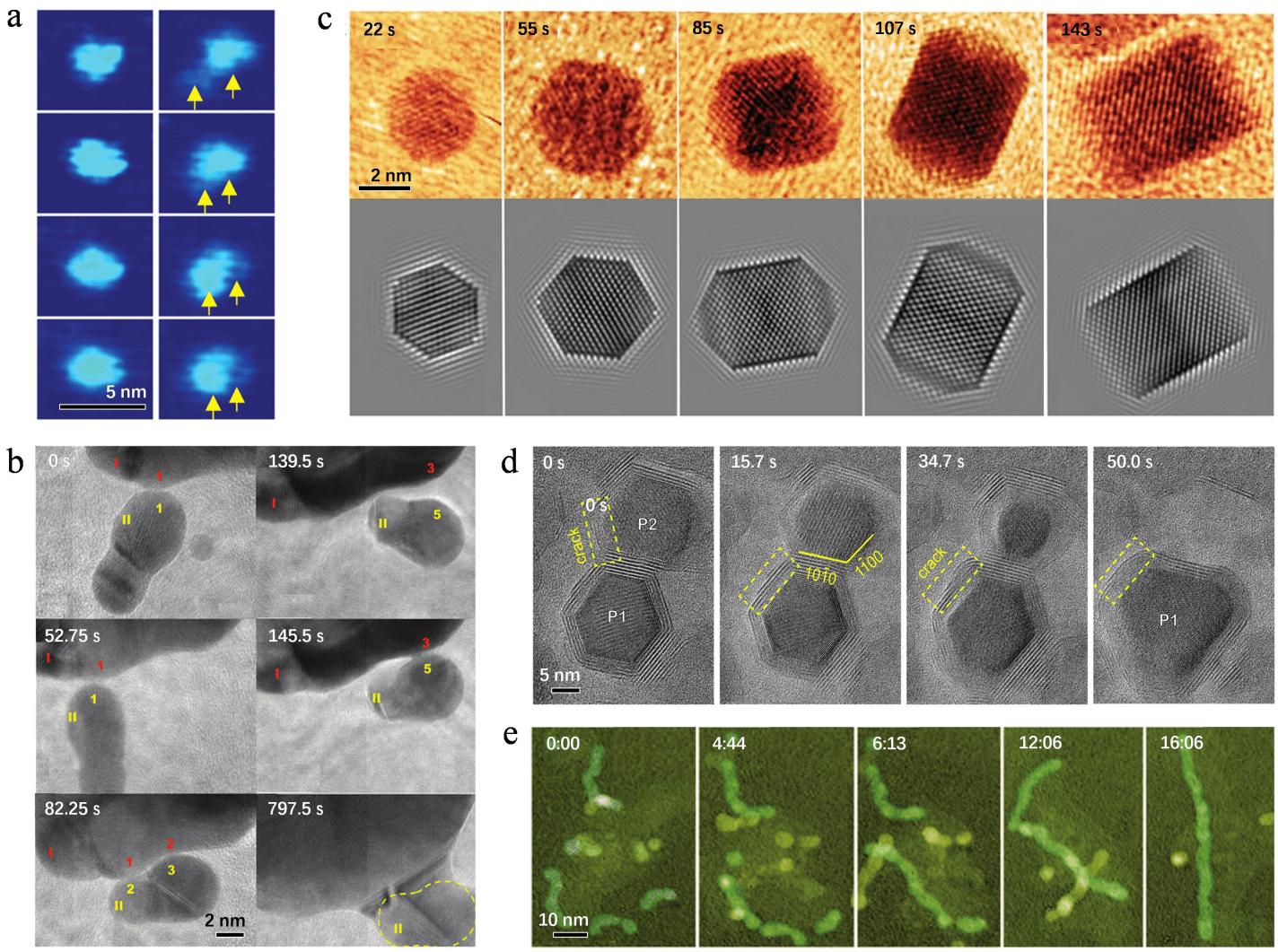

Figure 1. (a) Video images showing simple growth by means of monomer addition (first column) or growth by means of coalescence (second column). Particles are selected from the same field of view. Scale bar is 5 nm. Adapted from Zheng et al., Science, 10.1126/science.1172104 2009, AAAS [4]. (b) Sequence showing the typical dynamics of the attachment process. The surfaces of particles I and II make transient contact at many points and orientations (points 1-1, 1-2, 2-3, and 3-4) before finally attaching and growing together (point 3-5). The yellow dashed line indicates the original boundary of the attached particle. Scale bar is 2 nm. Adapted from Li et al., Science, 10.1126/science.1219643 2012, AAAS [8]. (c) Sequential images showing the growth of the Pt nanocube and simulated TEM images of the Pt nanoparticle. Scale bar is 2 nm. Adapted from Liao et al., Science, 10.1126/science.1253149 2014, AAAS [10]. (d) Sequential images showing the ripening process after two Cd–$CdCl_2$ core–shell particles are connected. P1 and P2 mark the two particles. Scale bar is 5 nm. Adapted from [12] under the Creative Commons Attribution 4.0 International License (CC BY 4.0). (e) Sequential color TEM images showing the growth of a long Pt_3Fe nanorod. Time is displayed as minutes:seconds, and the initial time is arbitrary. Nanorods and the specific particles serving as building blocks for nanorod formation are highlighted in green. Scale bar is 10 nm. Adapted from Liao et al., Science, 10.1126/science.1219185 2012, AAAS [14].

the oriented attachment of iron oxyhydroxide nanocrystals. Experimental results indicate that neighboring nanoparticles first achieve lattice alignment through rotational motion during Brownian motion, then undergo jump to contact driven by orientation-dependent Coulomb interactions, and ultimately coalesce into single-crystalline or twinned structures. Figure 1(b) shows the process. This study demonstrated that lattice alignment precedes particle fusion and highlighted the underlying kinetic factors driving the process—representing a significant advance in the understanding of non-classical crystal growth.

Xin and Zheng [9] further investigated the growth of Bi nanocrystals with LP-TEM. They observed both Ostwald ripening and reverse Ostwald ripening. Notably, they reported an oscillatory growth behavior of a single particle and revealed the mass-transport zone during the ripening process. This study provided

new kinetic insights into the maturation mechanisms of nanocrystals, offering a dynamic perspective that complements and extends classical growth models.

LP-TEM enables dynamic observation of the early nucleation and growth of nanomaterials. Through this observation, it reveals detailed processes, including the specific steps of nucleation and different growth pathways. These findings provide further support for traditional theories and help extend their scope.

With advancements in LP-TEM technology, the imaging resolution of LP-TEM has significantly improved, enabling deeper investigations of the behavior of nanomaterials in liquid environments. A landmark study reported by Liao *et al.* in 2014 [10] achieved atomic-scale observation of the growth of Pt nanocubes, allowing precise tracking of the evolution of individual crystal facets. Figure 1(c) shows the process of the growth. Their study revealed that, during the initial growth stage, all low-index facets of the Pt nanocrystals grew at similar rates, consistent with the Wulff construction. As the size of crystals increased, however, the 100 facets ceased growing due to the influence of surface ligands, ultimately leading to the formation of a cubic morphology. In parallel, nucleation studies have also deepened. For example, Loh *et al.* [11] discovered that nucleation in solution does not proceed directly from individual atoms to crystalline nuclei. Instead, the solution first undergoes spinodal decomposition, forming solute-rich and solute-poor liquid phases. Ordered crystal nuclei subsequently emerge within the solute-rich phase and grow via a bottom-up mechanism. This work provided critical insight into the intermediate stages of the nucleation process.

To gain a deeper understanding of nanomaterial growth mechanisms, extending studies beyond elemental noble metal nanocrystals to include complex systems such as core-shell structures and metal oxides is essential. Zhang *et al.* [12] conducted in situ LP-TEM observations of Cd-$CdCl_2$ core–shell nanocrystals using a self-designed carbon film based liquid cell. They discovered a unique, defect-mediated growth and maturation pathway for the core-shell structure: thermally induced fluctuations led to the formation of crack defects in the $CdCl_2$ shell, enabling mass transfer directly from core to core while the shell thickness remained nearly constant. Eventually, these defects healed, resulting in highly crystalline core-shell architectures. The process is shown in Figure 1(d).

In another study, Liang *et al.* [13] investigated the growth behavior of M–Fe–oxide (M=Ni, Mn, Co, or Zn) nanoparticles using LP-TEM. They found that the growth was limited by surface reaction and consistent with the Lifshitz–Slyozov–Wagner (LSW) model. Moreover, by comparing the nucleation behavior of different metal precursors, they observed that metals with similar reduction potentials (E_r) and thermal decomposition temperatures (T_d) were more likely to form mixed-metal oxides. This work offers new insights into the nucleation and growth mechanisms of metal oxide systems.

While the aforementioned studies primarily focus on nanoparticle growth, investigations into the growth of one-dimensional (1D) nanomaterials—such as nanorods and nanowires—as well as two-dimensional (2D) nanostructures also hold significant importance. Liao *et al.* [14] used LP-TEM to reveal a multistep growth mechanism for Pt_3Fe nanorods from nanoparticle building blocks: nanoparticles first underwent shape-directed end-to-end attachment to form curved polycrystalline chains, then transformed into single-crystal nanorods through straightening, orientational alignment, and mass redistribution. Figure 1(e) shows the process. In another study, Yang *et al.* [15] reported a unique growth pathway of transition metal oxide nanosheets evolving from 3D to 2D structures. Initially, 3D oxide nanoparticles form in solution; as size increases, the 3D nanoparticle transitions to 2D sheet driven by negative surface energy. Ye *et al.* [16] reported in situ visualization of molybdenum disulfide (MoS_2) nucleation and growth through chemical vapor deposition (CVD) by environmental transmission electron microscopy. They found when reached a critical size, MoS_2 underwent an in-plane structural ordering transition from amorphous structure into a crystalline nucleus. Furthermore, they captured oriented attachment and nuclei merging process during the primary stage. This work provides valuable insight into 2D single-crystal fabrication. These investigations into the growth of high-dimensional nanomaterials not only offer potential strategies for synthesizing nanostructures with controlled morphologies, but also provide in-depth insights into the complex thermodynamic and kinetic factors that determine anisotropic growth.

Overall, LP-TEM provides kinetic insights into the nucleation and growth of nanomaterials. It also complements traditional thermodynamic theories. In addition, LP-TEM reveals growth pathways from nanoparticles to complex systems and further to multidimensional nanomaterials. These advances

highlight the important role of LP-TEM in studies of nanomaterial nucleation and growth.

Although studies based on LP-TEM have greatly advanced understanding of nanomaterial growth processes and mechanisms, several challenges remain, including the limited understanding of complex-structured nanomaterials, and the lack of direct guidance for synthesizing multicomponent materials and hierarchical architectures. In addition, many current studies rely on electron beam to induce growth, which does not fully reflect the real solution environment. From a technical perspective, further improvements in the spatial and temporal resolution of LP-TEM are crucial for capturing atomic-scale dynamic behaviors in solution.

2.2 Etching and Corrosion

Etching is a powerful approach for regulating nanomaterial surface morphology that provides precise, flexible, and diverse methods for nanomaterial manufacture [17]. Meanwhile, corrosion of nanomaterials is widespread in electrochemical and catalytic processes and often has negative effects on their performance. The Wulff construction explains the morphological evolution of nanomaterials during etching and corrosion. However, real etching processes often occur in complex environments where multiple factors influence the final morphology. That makes it difficult for conventional ex situ techniques and classical theories to fully reveal the mechanisms. With high spatial and temporal resolution, liquid phase TEM enables direct visualization of complex intermediate states during etching, providing crucial insights into how multiple factors influence etching behavior and result [18–21]. These insights are crucial for precise morphological control of nanomaterials through etching and for reducing the negative impact of corrosion.

For the influence of complex factors on etching processes, Wang *et al.* [22] performed in situ LP-TEM studies of gold nanorod (AuNR) etching under different electron dose rates. At low dose rates, the morphological evolution of AuNRs was primarily thermodynamically driven, resulting in the formation of flattened facets at the rod ends. At intermediate dose rates, the etching rate correlated with surface curvature—the higher the curvature, the faster the etching. This led to a shape transition from rod-like to ellipsoidal, followed by complete dissolution. Under high electron dose rates, a blurry shell composed of dissolved Au^{3+} species formed around the AuNR surface, further promoting sidewall corrosion and producing a thinner, more elongated intermediate morphology. These processes are shown in Figure 2(a). By quantitatively comparing the relationship between nanorod dimensions and etching rate under different conditions, the study also revealed that smaller AuNRs etched more rapidly at low dose rates, while the size effect diminished at higher doses. These findings provided mechanistic insights into the rate-dependent etching behavior.

In the following study, Wang *et al.* [23] investigated the influence of dissolved O_2 bubbles on the etching behavior of AuNRs. They found that the presence of O_2 significantly accelerated the etching process, and when the distance between the gas bubble and the nanorod decreased below a critical threshold (1 nm), the etching rate near the bubble increased sharply, as shown in Figure 2(b). This work revealed the unique reaction dynamics at complex solid-liquid-gas interfaces.

Zhang *et al.* [24] used in situ TEM (in vacuum) to examine how surface ligands influence the etching of Ag_2O_2 nanocrystals. By comparing the morphological evolution of Ag_2O_2 with and without ligands, they discovered that ligands lead to pinning effect, protecting the underlying crystal from etching. However, as etching proceeded on ligand-free facets, the remaining crystal beneath the ligand eventually dissolved. Figure 2(c) shows that the etching process can be divided into three regimes: spherical-to-cuboidal shape transformation, side etching, and bottom etching. While this study was not conducted in liquid phase, it offers valuable mechanistic insight into ligand mediated etching and highlights opportunities for constructing complex nanostructures via selective facet protection.

Ye *et al.* [25] observed morphological evolution of single anisotropic gold nanocrystals under a controlled redox environment in a graphene liquid cell. This study provides crucial insights into the relationship between nanocrystal morphologies and kinetically stabilized surface features.

Hauwiller *et al.* [18] further explored environmental factors influencing etching behavior using graphene liquid cells preloaded with $FeCl_3$ and electron beam-induced radiolysis products (mainly ·OH and H_2O_2). By studying the etching of gold nanocrystals under these chemically complex conditions, they found that the electron beam primarily regulated the total oxidant concentration in solution, which

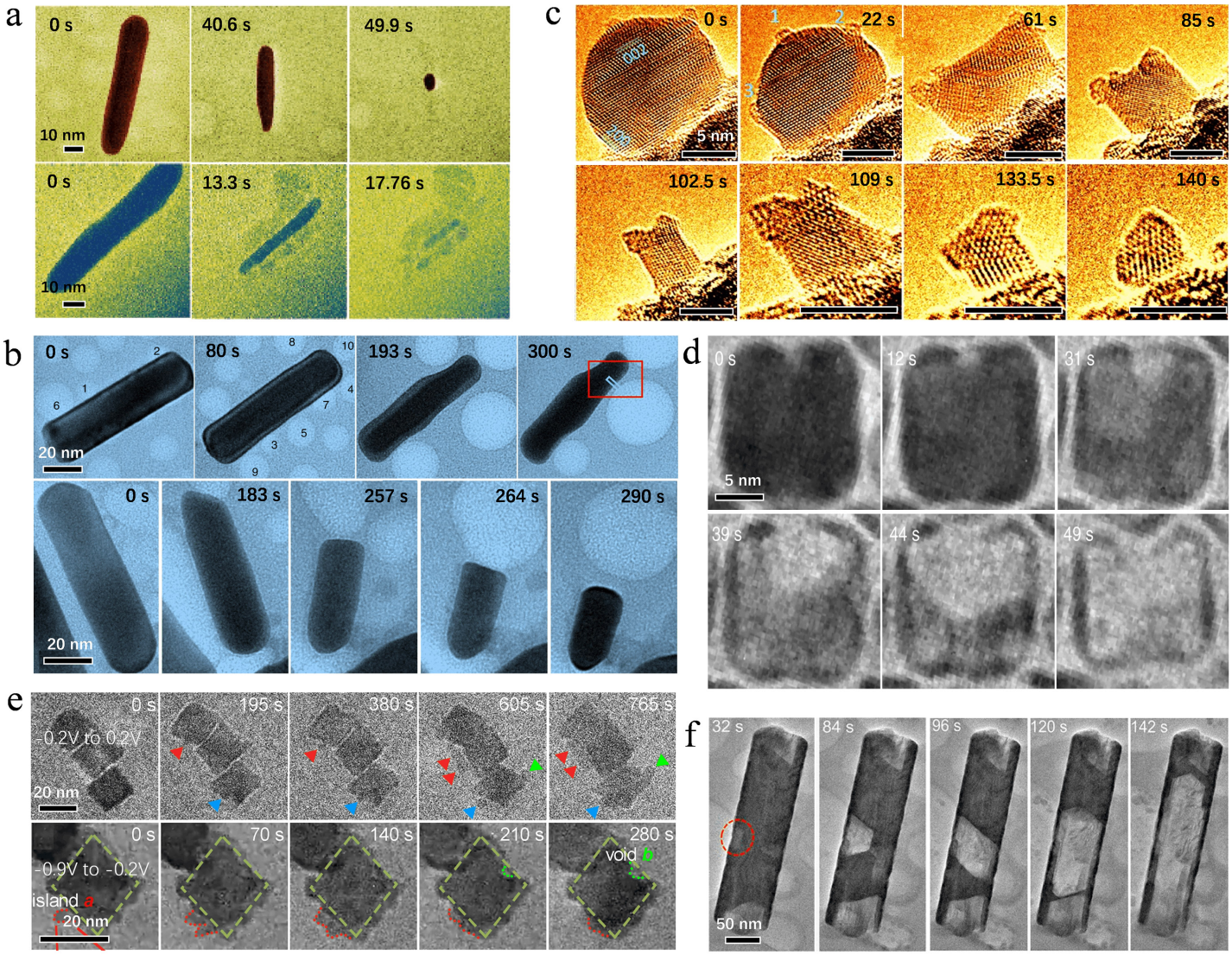

Figure 2. (a) Sequential TEM images show the morphology evolution of a nanorod under the dose rate of $1.5 \times 10^{10}\,\mathrm{Gy\,s^{-1}}$ and $4.5 \times 10^{10}\,\mathrm{Gy\,s^{-1}}$. Scale bar is 10 nm. Adapted from [22]. (b) Time-sequential TEM micrographs showing real-time shape evolution of the Au nanorod during etching. Scale bar is 20 nm. Adapted from [23]. (c) Sequential HRTEM images (false color) show the real-time shape evolution of the Ag_2O_2 nanocrystal with Ag surface adsorbates during etching under an electron beam. Scale bar is 5 nm. Adapted from Zhang et al., Nano Lett., 2019, DOI:10.1021/acs.nanolett.8b04719, ACS [24]. (d) Time sequential TEM micrographs showing the etching process of internal Pd atoms in a single terrace defected Pd@Pt cube. Scale bar is 5 nm. Adapted from [26] under the Creative Commons Attribution 4.0 International License (CC BY 4.0). (e) Time-sequential in situ TEM images of morphological evolution under the CV from -0.2 V to 0.2 V and from -0.9 V to -0.2 V vs. Pt. The red and green dotted areas are named Island a and Void b, respectively. Scale bar is 20 nm. Adapted from [27] under the Creative Commons Attribution 4.0 International License (CC BY 4.0). (f) Sequential TEM images showing the etching process at a dose rate of 1210 $e^{-}\mathrm{\AA}^{-2}s^{-1}$. Scale bar is 5 nm. Adapted from [28] under the Creative Commons Attribution 4.0 International License (CC BY 4.0).

affected the overall etching rate, while $FeCl_3$ influenced the relative proportion of oxidative species and thus the chemical potential driving the reaction. This study decoupled the roles of different chemical parameters in etching and opened new avenues for controllable, etching-based morphology engineering of nanomaterials.

In studies of corrosion processes, Shan *et al.* [26] reported an electrochemical LP-TEM investigation of the dynamic corrosion pathways of Pd@Pt core–shell nanocubes (Figure 2(d)). The study revealed a corrosion process that slow galvanic etching occurring at defect-free sites proceeds in parallel with fast defect-mediated halogen-induced etching, with the two processes mutually constraining each other. The results also showed that the edges

and corners of the nanocubes were etched first. Subsequently, this group used electrochemical LP-TEM to observe the transformation of Pd@Pt core-shell octahedral nanoparticles into Pt nanoframes during corrosion [27]. By employing cyclic voltammetry to simulate realistic electrochemical corrosion environments, the study revealed a potential-dependent surface reconstruction process. It was found that the corrosion process consists of two components: etching and redeposition of Pd, and preferential corrosion of step sites on Pt(111) facets (Figure 2(e)). Furthermore, the site-specific atomic dynamics of Pt and Pd were attributed to oxidation and reduction processes. In later work, Peng *et al.* [28] used high-resolution LP-TEM to directly observe the corrosion behavior of Sn nanocrystals with and without Ni_3Sn_4 surface layers. During the corrosion of Sn@Ni_3Sn_4 nanocrystals, pitting corrosion first occurred at defect sites in the protective layer, followed by a transition from isotropic etching to facet-dependent etching, ultimately leading to the formation of hollow structures that terminated at low-index facets (Figure 2(f)). In the absence of a protective layer, Sn nanocrystals exhibited uniform corrosion and smooth surfaces at high etching rates, whereas rough surfaces formed at lower etching rates. This study provides detailed insights into the effects of defects and surface coatings on corrosion behavior.

In addition, one of the key advantages of LP-TEM is the ability to enable quantitative studies of etching and corrosion processes based on high spatiotemporal resolution imaging data. Wu *et al.* [29] employed LP-TEM to monitor the etching behavior of Pt nanocrystals with different shapes in $HAuCl_4$ solution, and quantitatively analyzed the correlation between atomic site position within the crystal—namely, corner (0D), edge (1D), and terrace (2D) sites—and the corresponding etching rates.

$$r^{3-k} - r_0^{3-k} = -N_k A_k t, \quad k \in \{0, 1, 2\} \qquad (1)$$

where k denotes the atomic site type—corner ($k = 0$), edge ($k = 1$), and terrace ($k = 2$); r represents the size of the nanocrystal; A_k is a shape-dependent etching coefficient; and N_k is a dimensionality-dependent factor related to the number of etching sites. The study revealed that the etching rate at different atomic positions follows a power-law relationship, with etching rates differing by orders of magnitude among atoms at different sites. This work quantitatively revealed the relationship between etching rate and atomic position, highlighting the importance of the high-resolution imaging ability of LP-TEM.

In summary, LP-TEM enables nanoscale dynamic observation of nanomaterial etching and corrosion behaviors. It not only analyzes the factors that affect etching and corrosion from a kinetic perspective, but also provides methods for quantitative analysis.

2.3 Self-Assembly

Self-assembly of nanomaterials is when nanoscale building blocks, such as nanoparticles, nanowires, and nanosheets, assemble into ordered structures by physical or chemical forces. In this process, preformed nanoparticles spontaneously organize into long-range ordered structures, such as superlattices, colloidal crystals, or stable shapes driven by non-covalent interactions. These non-covalent interactions include van der Waals forces, electrostatic forces, and hydrogen bonding. These assembled structures typically have unique properties. Self-assembly is also expected to become a bottom-up strategy for constructing complex nanostructures. Understanding the interparticle interactions and colloidal stability is crucial for controlling the self-assembly process. According to the Derjaguin-Landau-Verwey-Overbeek (DLVO) theory, the total interaction between colloidal particles is the linear sum of van der Waals attraction and electrical double-layer repulsion, with the net potential determining their assembly stability. However, at the nanoscale, ion size effects, ion-ion interactions, ion-ion correlations [30], and the structuring of water [31] cause short-range structural forces and ion association effects, leading to the breakdown of DLVO predictions. Furthermore, beyond interparticle forces, factors such as particle anisotropy [32] and hydrophobic interactions also significantly influence self-assembly behavior, though probing their roles remains highly challenging.

LP-TEM offers powerful methods for visualizing the self-assembly of nanoparticles in solution with atomic-scale resolution. It enables direct observation of assembly pathways and mechanistic insights inaccessible to other characterization tools. In studies of interactions between nanomaterials, Chen *et al.* [33] quantitatively investigated the interaction potentials between nanocrystals by analyzing their relative motion trajectories obtained from LP-TEM. This study observed that gold nanorods preferentially assemble in a tip-to-tip fashion in solution, owing to a long-range and highly anisotropic electrostatic repulsive interactions, in contrast to the side-by-side

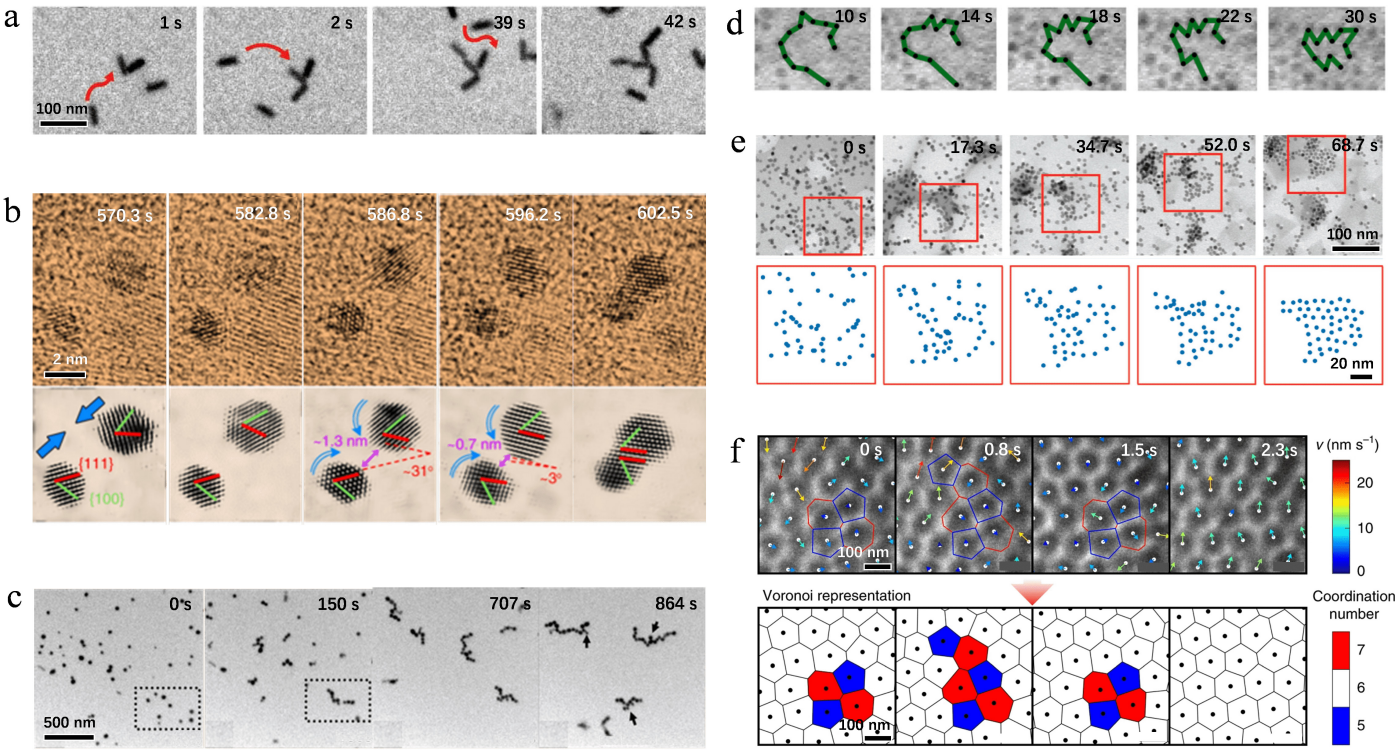

Figure 3. (a) A time series of TEM images showing how nanorods approach and attach to each other. Red arrows highlight the trajectories of nanorods before they attach to the cluster of growing rod assemblies. Scale bar is 100 nm. Adapted from [33]. (b) Imaging of OA at atomic level shows the OA process of small gold nanoparticles at 111 surface, evolving into a twin structure. The sequences below each false-color TEM image are corresponding filtered images that highlight the evolution of particle orientations during OA, and also show the approaching of particles and the establishment of pre-alignment by rotation, after which the jump to contact occurs. Red lines stand for 111 facets and green ones for 100 facets. Dashed lines depict the relative angle between the 111 facets of the two particles. The direction of movement of the particles (approaching and rotation) is denoted by blue arrows. Scale bar is 2 nm. Adapted from [34] under the Creative Commons Attribution 4.0 International License (CC BY 4.0). (c) The time-sequential images of the assembly process. At the beginning, NPs are well separated; after 150, s illumination by an electron beam with an intensity of 10, pA, cm^{-2}, dimers and trimers form, followed by short chains produced through the attachment of existing dimers, trimers, and individual NPs. The scale bar is 500 nm. Adapted with permission from [35]. Copyright 2013 American Chemical Society. (d) Dynamics of nanoparticles aligned in one-dimensional chains. The time-sequential images shows chains formed at the beginning of assembly, where particle connectivity is tracked over time to illustrate folding and clumping behavior. Adapted with permission from [36]. Copyright 2016 American Chemical Society. (e) In situ observation of superlattice formation by liquid phase TEM and lattice-gas modeling. The first row shows TEM snapshots at different times. The scale bar is 100nm. The second row shows relative positions (corrected for thermal drift of the TEM sample) of selected 51 NPs taken from the red-squared area (120 nm × 120 nm) in the first row. The scale bar is 20 nm. Adapted with permission from [37]. Copyright 2012 American Chemical Society. (f) Time-lapse liquid phase TEM images and corresponding Voronoi representations of the lattice, showing the annealing of imperfectly coordinated sites. The color of each cell denotes the coordination number. Arrows in the top panel are colored by the magnitude of the instantaneous velocity of individual columns v, calculated from successive TEM images. Scale bars for all images are 100 nm. Adapted from [38].

arrangement typically observed in dry environments (Figure 3(a)). This study not only clarifies the complex interactions involved in nanocrystal assembly but also provides a potential approach for the quantitative investigation of nanoscale interactions. For instance, Zhu *et al.* [34] used LP-TEM to study the driving forces controlling oriented attachment of gold nanoparticles in solution. They observed that as two nanoparticles approached one another, they initially rotated randomly. Upon ligand shell overlap, their motion transitioned into directional rotation. Once crystallographic alignment was achieved, nanoparticles made contact, accompanied by ligand desorption (Figure 3(b)). This study clarified the role of surface ligands in the self-assembly of nanoparticles. These LP-TEM-based studies reveal additional interactions and factors that govern nanoparticle self-assembly. These findings provide an

effective complement to DLVO theory by extending its description of assembly behavior.

Recent studies based on LP-TEM have successfully captured the self-assembly of nanoparticles into structures ranging from one-dimensional (1D) to three-dimensional (3D) configurations.

In the case of 1D assembly, Liu *et al.* [35] employed LP-TEM to investigate the electron-beam-induced self-assembly behavior of Au nanoparticles modified with either cetyltrimethylammonium (CTA^+) or citrate ions in aqueous solution (Figure 3(c)). They found that when the electron beam intensity exceeded 5 pA cm^{-2}, positively charged nanoparticles assembled into 1D chain-like structures, whereas negatively charged particles remained stationary under all beam intensities. The mechanism was attributed to the electrostatic repulsion between like-charged particles; hydrated electrons (eaq^-) generated by the electron beam neutralized the surface charge of CTA^+-coated particles, thereby reducing repulsion. Dipole-dipole interactions subsequently drove particles into linear chains. This work not only demonstrated a beam-mediated method for constructing 1D nanoparticle chains, but also provided insights into the complex mechanisms determining the self-assembly of charged nanoparticles.

For 2D assembly, Powers *et al.* [36] studied the self-assembly of superparamagnetic $PtFe_3$ nanoparticles and uncovered a distinctive two-stage mechanism. Initially, long-range anisotropic magnetic forces led to the formation of 1D linear chains, which subsequently folded and compacted into dense, 2D aggregates dominated by short-range van der Waals interactions. In this process, long-range magnetic forces significantly accelerated nanoparticle aggregation (Figure 3(d)). By visualizing the intermediate assembly states, this study not only identified a novel pathway of structural evolution but also highlighted the role of non-DLVO interactions in nanoparticle self-assembly, extending classical colloidal theory.

Park *et al.* [37] used LP-TEM to study the self-assembly of Pt nanoparticles during solvent evaporation in a mixed organic solution. They observed a unique assembly process (Figure 3(e)) that in the first stage, receding solvent fronts dragged nanoparticles together and condensed them into amorphous agglomerates. In the second stage, local solvent fluctuations relaxed the system into an ordered 2D superlattice. Furthermore, they demonstrated that the superlattice could continue to grow through the addition of single nanoparticles after the crystallization event. This study revealed a drying-mediated assembly mechanism that crystallization occurred after the nanoparticles formed a dense disordered phase, with particle motion driven by solvent fluctuations and capillary interactions while Brownian motion is significantly suppressed.

For 3D assembly, Ou *et al.* [38] employed LP-TEM to study the assembly of dispersed gold nanoprisms into superlattices at the single-particle level (Figure 3(f)). They revealed the structural evolution from orientational disorder to an ordered superlattice. Chen *et al.* [39] investigated the self-assembly kinetics of Janus spheres with hemispherical hydrophobic attraction. They found that small, kinetically favored isomers could fuse before reaching equilibrium to form highly ordered fibrillar triple helices, indicating that chemical anisotropy and reaction kinetics jointly govern the formation of ordered structures.

By enabling atomic-scale imaging of nanomaterial self-assembly, LP-TEM reveals not only interactions that drive the assembly process, but also the formation pathways of nanostructures from 1D to 3D architectures.

Despite these advances, studies of nanoparticle self-assembly based on LP-TEM still face several limitations, including constrained spatial resolution and limited control over reaction environments. Addressing these challenges will be essential in future research.

3 LP-TEM Studies for Nanoscale Electrochemical Applications

LP-TEM has been widely applied by researchers owing to its strong capability for dynamic observation [40–43]. Nano electrochemistry is one of the important application fields of LP-TEM, and by integrating electrodes into a liquid cell to construct an electrochemical liquid cell, dynamic observation of nano electrochemical behavior can be achieved. Due to their high energy density, long cycle life, and low memory effect, lithium-ion batteries have long been a focus of research in the field of electrochemical energy storage. However, significant challenges are still faced in practical applications of lithium-ion batteries, such as the uncontrolled growth of lithium dendrites, and the difficulty in understanding the mechanism of solid electrolyte interphase (SEI) formation, which can lead to short lifetime of batteries. LP-TEM allows direct atomic-scale visualization of

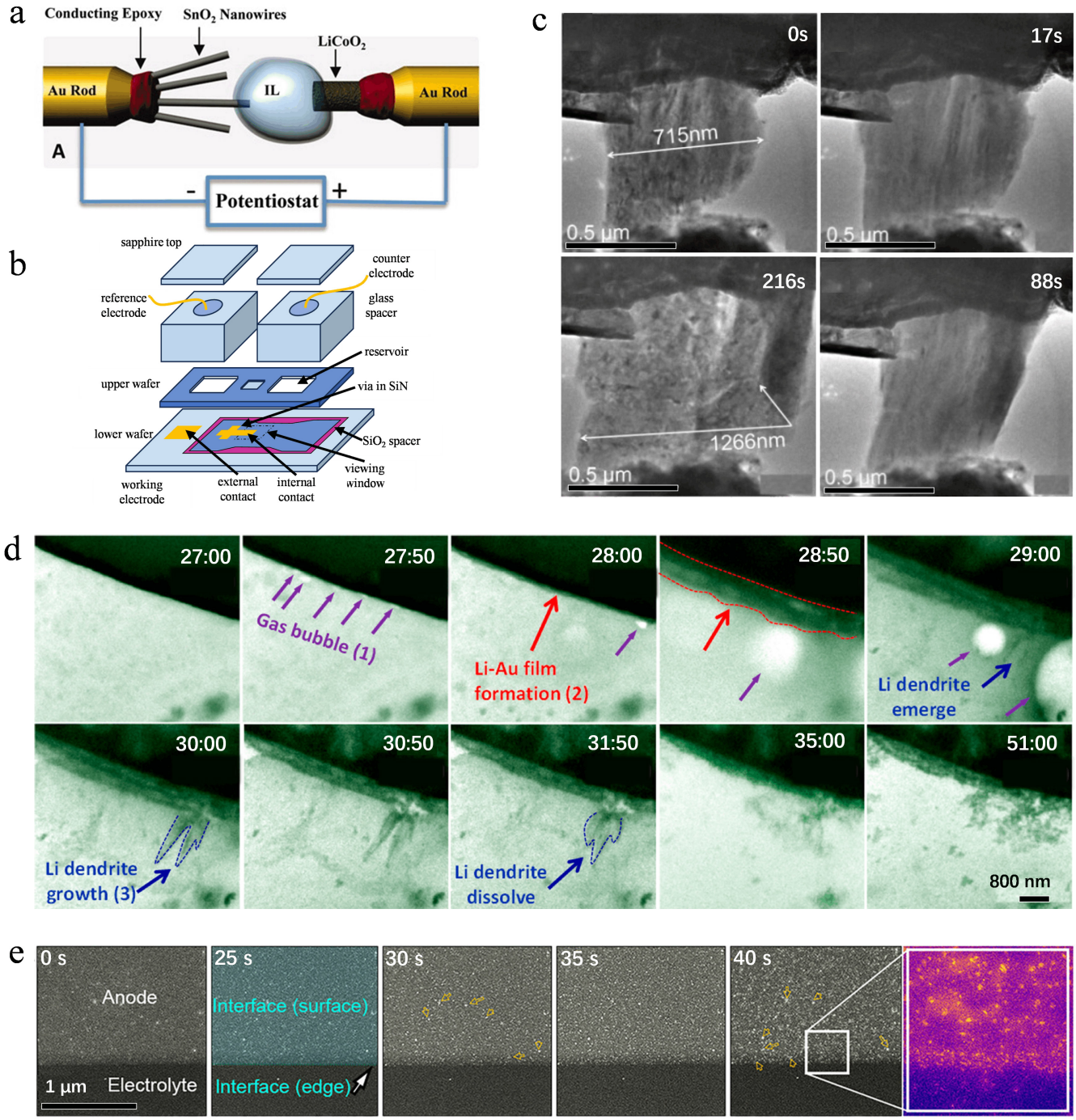

Figure 4. (a) Schematic of the open liquid-cell model developed by Huang *et al.*. Adapted from Huang *et al.*, Science, 10.1126/science.1195628 2010, AAAS [44]. (b) Components of the cell developed by Williamson *et al.*. The viewing window is enlarged for clarity. Adapted from [46]. (c) Time-resolved TEM images extracted from video frames showing the microstructure evolution of the BP sheet during the first cycle, including the pristine BP sheet, the charging process, and the discharging process. Anode cracking and pulverization accompanied by a large volume expansion appear during the delithiation process, which is significantly different from the commonly accepted understanding. A typical magnified TEM image of the delithiated anode shows obvious cracking. Scale bar is $0.5\,\mu\mathrm{m}$. Adapted with permission from [47]. Copyright 2016 American Chemical Society. (d) Time evolution of the growth and dissolution of Li–Au alloy and lithium dendrites. Scale bar is $800\,\mathrm{nm}$. Adapted from [48]. (e) Time evolution of the GC–electrolyte interface during cycling. A time-lapse series of ADF-STEM images of the GC–electrolyte interface shows the growth of the SEI during cycling. Scale bar is $1\,\mu\mathrm{m}$. Adapted from [51] under the Creative Commons Attribution 4.0 International License (CC BY 4.0).

dynamic interfacial processes between electrodes and electrolytes in lithium batteries, offering crucial insights into underlying reaction mechanisms and providing a powerful tool to overcome the technological bottlenecks associated with lithium battery performance and safety.

To enable TEM investigations of internal interfacial behavior in batteries, researchers have developed various types of nano electrochemical platforms, including open-cell and sealed liquid cell. As early as 2010, Huang *et al.* [44] introduced an in situ TEM approach based on an open cell to study electrochemical behavior at the nanoscale. This open electrochemical cell consisted of a SnO_2 nanowire anode, a bulk $LiCoO_2$ cathode, and an ionic liquid electrolyte (Figure 4(a)). Owing to the low vapor pressure of the ionic liquid under vacuum, the cell did not require a closed window, allowing for high-resolution imaging. However, ionic liquids differ significantly from commercial battery electrolytes, thereby reducing the relevance to realistic battery environments.

Subsequently, Zhong *et al.* [45] developed another type of open nano electrochemical device, comprising a lithium metal anode, anatase TiO_2 nanowire cathode, and a solid Li_2O electrolyte layer. They tracked the lithiation pathway of individual anatase TiO_2 nanoparticles. This study found that when the particle diameter was below 25 nm, the lithiation mechanism transitioned from a two-phase to a single-phase reaction. However, this configuration is only applicable to systems with solid electrolytes and is not suitable for studying liquid-electrolyte-based batteries.

To better simulate the working environment of practical batteries, many studies have adopted sealed liquid cells. In 2003, Williamson *et al.* [46] conducted one of the earliest studies in this area, using a SiN_x liquid cell to investigate the electrodeposition of Cu on an Au electrode (Figure 4(b)). This work is a landmark of electrochemical studies using LP-TEM. The study achieved high temporal resolution imaging as 30 frames per second of the solid-liquid interface, enabling real-time observation of Cu cluster nucleation and growth. It showed the feasibility of using sealed liquid cells for studying electrochemical interactions under realistic conditions and paved the way for subsequent LP-TEM studies of dynamic solid-liquid interfacial processes.

Beyond electrochemical deposition, electrochemical stripping is also a key process in the charge-discharge cycles of lithium-ion batteries, particularly relating to electrode delithiation. Xia *et al.* [47] reported a study of lithiation and delithiation of black phosphorus (BP), a layered anode material, under vacuum conditions (Figure 4(c)). They observed significant volume expansion and cracking during the delithiation process, along with the formation of Li_3P. These morphological and chemical transformations were identified as major contributors to the failure of BP anodes.

The uncontrolled growth of lithium dendrites and the formation of the solid electrolyte interphase (SEI) at the electrode-electrolyte interface during charge-discharge cycles are critical factors limiting the lifetime and safety of lithium-ion batteries. These two processes have long been a focus in battery research. Zeng *et al.* [48] employed sealed liquid cell firstly in situ observed the dynamic interfacial processes between a commercial electrolyte ($LiPF_6$ in EC/DEC) and a gold electrode. Specifically, they observed inhomogeneous lithiation, lithium metal dendrite growth, electrolyte decomposition, and SEI formation (Figure 4(d)). This study successfully established a sealed liquid cell incorporating a low-vapor-pressure commercial electrolyte, showing the feasibility of using LP-TEM to study realistic electrolyte systems.

Leenheer *et al.* [49] also used a sealed liquid cell with a commercial electrolyte to investigate lithium deposition and stripping under constant current conditions. They observed that the electron beam induced the formation of solid SEI layers, thereby altering the kinetics of lithium growth. In another study, Sacci *et al.* [50] further investigated SEI formation and evolution by in situ ec-S/TEM. They reported that the density of SEI is twice that of the electrolyte. In addition, they found Li nucleation and growth on the site-specific locations of the surface and edges of the glassy carbon electrode.

With advances in imaging resolution, LP-TEM has enabled more detailed investigations of battery interfaces. Dachraoui *et al.* [51] employed operando electrochemical liquid phase scanning transmission electron microscopy (EC-STEM) to visualize the real-time dynamics at the electrode–electrolyte interface. They provided a detailed mechanistic view of SEI formation consistent with the mosaic model (Figure 4(e)): initial electrolyte decomposition during the first charge leads to the nucleation of inorganic nanoparticles, followed by the formation of discrete

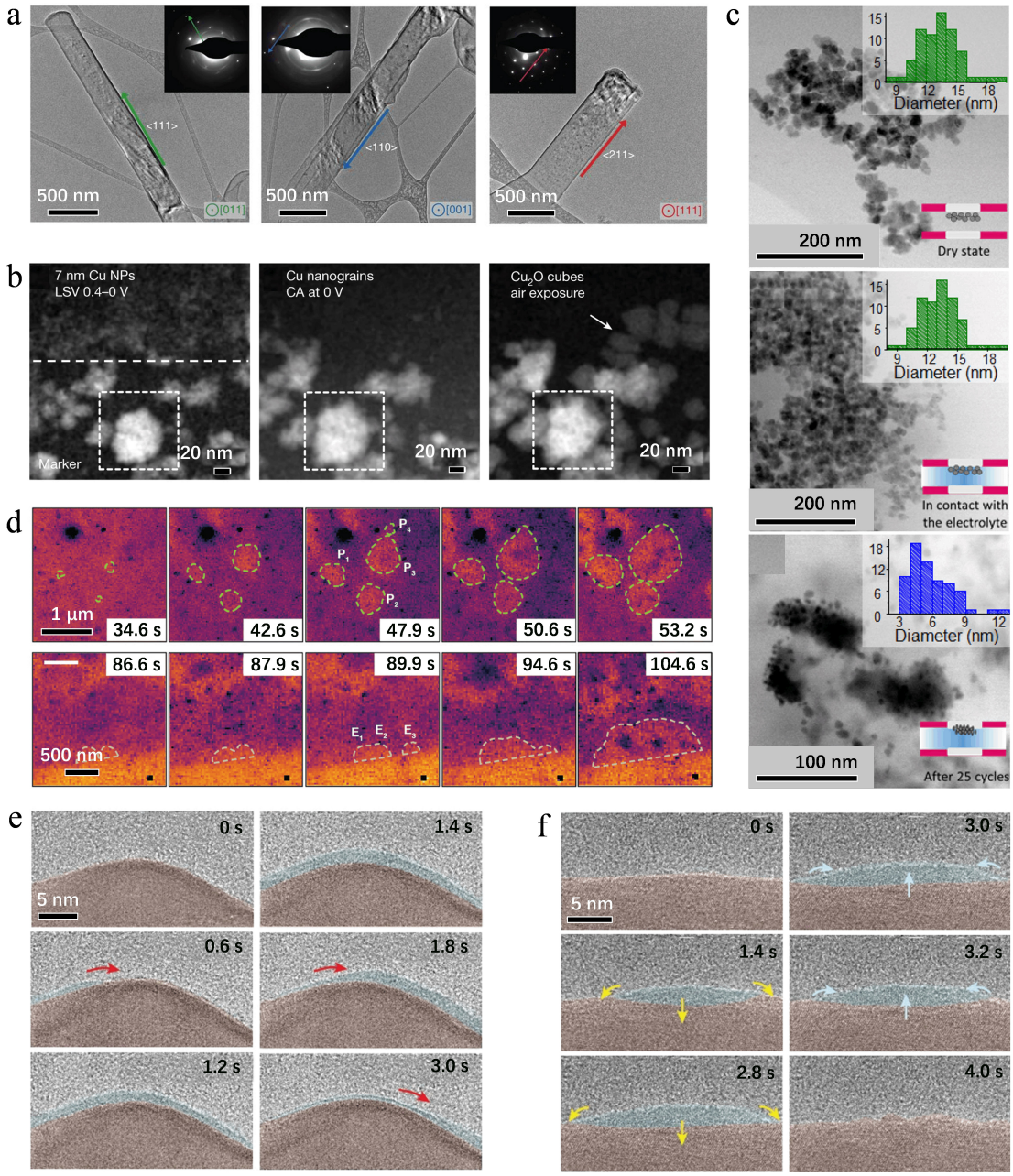

Figure 5. (a) Li metal dendrites and their corresponding SAED patterns (insets) growing along ⟨111⟩, ⟨110⟩, and ⟨211⟩. The electron dose rate is $< 1\, e^{-}\ \text{Å}^{-2}\ \text{s}^{-1}$ for approximately 30 s. Scale bar is 500 nm. Adapted from Li et al., Science, 10.1126/science.aam6014 2017, AAAS [52]. (b) Overview of the life cycle of 7 nm Cu nanocatalysts shown by EC-STEM images, including the initial growth after a single negative-direction LSV scan from 0.4 to 0 V, further growth under CA at 0 V, and the post-electrolysis formation of Cu_2O cubes (marked by the arrow) when exposed to air at the same location. Scale bar is 20 nm. Adapted from [55]. (c) In situ STEM images of Co_3O_4 nanoparticles deposited over the glassy carbon electrode in the observation window of the electrochemical TEM sample holder: particles as prepared in the dry state, in contact with a 0.1 M KOH electrolyte before electrochemical measurements, and after 25 voltammetric cycles from 0.6 to 1.8 V vs. RHE in a 0.1M KOH aqueous electrolyte at $20\ \text{mV}\ \text{s}^{-1}$. Top insets show the corresponding size distributions, while the lower insets schematize the in situ EC-TEM cell and the location of the sample on the cell window. Scale bar is 20 nm. Adapted with permission from [56]. Copyright 2019 American Chemical Society. (d) LP-TEM images of H_2 bubble growth at point defects (P1–P4) and edge sites (E1–E3), respectively. Contours of the gas–liquid–solid interfaces are indicated by dashed lines. Time-dependent contour lines are displayed on the right side of the images. Scale bars: 1μm in the first row and 500 nm in the second row. Adapted from [57]. (e) HRTEM images showing the liquid-like flow of the amorphous phase on the crystalline Cu surface. Scale bar is 5 nm. Adapted from [58]. (f) HRTEM images showing the interconversion between crystalline Cu and the amorphous interphase. Scale bar is 5 nm. False colours are used to guide the eye. Adapted from [58].

island layers, then deposition of organic species, ultimately forming a dense composite structure of organic matrix embedded with inorganic domains. This work offers a powerful platform for future operando studies of battery interfacial chemistry.

In the study of lithium dendrites and SEI films, achieving atomic-resolution imaging using LP-TEM remains challenging due to the beam sensitivity and low atomic number of these materials. To overcome this limitation, cryogenic electron microscopy (cryo-EM) has been introduced to the investigation of lithium battery interfaces. By rapidly freezing the samples, cryo-EM significantly enhances their tolerance to electron beam irradiation. In 2017, Li *et al.* [52] employed cryo-EM to image lithium dendrites and SEI layers at atomic resolution (Figure 5(a)). They revealed that lithium dendrites possess a single-crystalline structure and preferentially grow along the <111> crystallographic direction. Additionally, their study demonstrated that SEI morphology varies significantly depending on the electrolyte chemistry.

Further contributions by Meng's group [53] using cryo-EM confirmed the presence of an amorphous phase during the early stages of lithium dendrite growth, supplementing previous structural observations. Their group later extended their investigations to study inactive lithium species in lithium batteries [54]. They quantified the metallic Li^0 content and found that the majority of inactive lithium consists of unreacted metallic Li^0 rather than Li^+ species incorporated into the SEI.

Although cryo-EM lacks the capability to dynamically monitor interfacial reactions, its ability to deliver high-resolution structural and morphological information makes it a valuable complement to in situ LP-TEM. Together, these techniques provide a more comprehensive view of interfacial processes in lithium batteries, spanning both dynamic behavior and static atomic-scale structure.

In addition to probing dynamic interfacial processes in batteries, LP-TEM has also become a powerful tool for investigating electrocatalytic reactions. Among the most representative reaction systems in contemporary electrocatalysis are the CO_2 reduction reaction (CO_2RR), hydrogen evolution reaction (HER), and oxygen evolution reaction (OER), all of which play critical roles in carbon-neutral technologies and clean energy production.

Recently, Yang *et al.* [55] employed operando electrochemical liquid phase scanning transmission electron microscopy (EC-STEM) in combination with four-dimensional STEM (4D-STEM) to study the life cycle of Cu catalysts under realistic CO_2RR conditions (Figure 5(b)). They discovered that the Cu nanoparticles were highly polycrystalline, with grain boundaries serving as abundant active sites and the primary source of catalytic activity. By capturing the behavior of Cu catalysts under working CO_2RR conditions, this study resolved longstanding debates regarding the active valence state of Cu and highlighted the power of LP-TEM in elucidating electrocatalytic mechanisms.

Ortiz Peña *et al.* [56] used LP-TEM to study behavior of Co_3O_4 nanoparticles during OER catalysis and revealed an irreversible surface amorphization process that correlated positively with the alkalinity of the electrolyte (Figure 5(c)). Meanwhile, Kim *et al.* [57] investigated HER on MoS_2 surfaces and observed that gas bubbles nucleated sequentially at strain defects, point defects, and edge sites (Figure 5(d)). At high negative potentials, a liquid film channel formed between the bubble and catalyst surface, sustaining continuous hydrogen evolution. Notably, this study employed deep learning-based image denoising techniques to enhance TEM image resolution, illustrating the growing role of AI in advancing LP-TEM research.

In addition, Zhang *et al.* [58] used a self-developed polymer-based electrochemical liquid cell for TEM to achieve atomic-scale in situ observation of the dynamic behavior of charged solid–liquid interfaces during Cu-catalyzed CO_2 electroreduction (CO_2ER) (Figure 5(e, f)). They identified a fluctuating amorphous intermediate layer with liquid-like characteristics that can reversibly transform between crystalline and amorphous states, flow along the charged Cu surface, and induce surface reconstruction and material loss of crystalline Cu. Combined with theoretical calculations, this study elucidated a charge-activated electrolyte–surface reaction mechanism that drives amorphous surface reconstruction, providing important insights into the dynamic evolution of electrochemical interfaces.

In summary, LP-TEM has achieved milestone advances in the field of electrochemical research, providing deep insights into the evolution of solid-liquid interfaces in batteries and the structural reconstruction of electrocatalyst surfaces. Recent studies highlight

a growing trend toward real-time monitoring of electrochemical reactions under operando conditions, which is becoming increasingly central to nanoscale electrochemistry. Nevertheless, current LP-TEM approaches still face limitations when applied to complex, realistic electrochemical environments. Future efforts must focus on the development of next-generation electrochemical liquid cells to overcome these challenges and further expand the capabilities of in situ electrochemical studies.

4 Conclusions and Outlooks

LP-TEM has become an indispensable tool for characterizing dynamic processes of nanomaterials and has realized great achievements in revealing nonclassical nucleation and growth pathways, complex etching and assembly dynamics, and the mechanisms underlying electrochemical processes. However, LP-TEM still faces several challenges.

In terms of spatial resolution, the combined thickness of the liquid layer and the liquid cell windows makes liquid samples thicker than those in vacuum. Additionally, the beam sensitivity of samples limits the electron dose rate during imaging. These factors collectively constrain the spatial resolution of LP-TEM. Recent LP-TEM studies based on carbon-film liquid cells have substantially improved the spatial resolution; however, the imaging resolution remains limited under complex and more realistic operando conditions. For instance, it is still difficult to achieve a high-resolution visualization of nanoparticle dynamics under electric fields.

In terms of environmental control, the design of liquid cells is constrained by multiple factors, including spatial confinement, electron beam effects, and imaging resolution. As a result, the experimental environment inside the liquid cell often differs from the real conditions. Moreover, precise control over key parameters such as liquid layer thickness, temperature, electric field, and illumination within the cell remains challenging. The integration of multiple external fields (multiphysics coupling) into the liquid cell environment is still limited, thereby narrowing the applicable scope of LP-TEM and restricting its ability to investigate nanomaterials in complex real-world systems. For example, studies on thermal effects in batteries require in situ liquid-phase chips capable of coupling electric and thermal fields, which remains a challenge under current experimental conditions.

In terms of electron beam effects, the imaging process can interfere with the intrinsic physicochemical processes of the sample. On one hand, the electron beam interacts with certain liquid solvents and induces radiolysis of water, generating reactive species such as free radicals. These radiolysis byproducts can alter the chemical environment of the solution and, in turn, affect processes such as nanomaterial growth and deposition, leading to deviations from behavior under realistic conditions. Recent studies have adopted strategies to reduce electron-beam effects; however, in future liquid cells with multi-field control, it will remain a nonnegligible factor. Minimizing beam-induced effects remains a major challenge in LP-TEM research.

To address the aforementioned challenges, this review provides outlooks for LP-TEM studies. Future research should focus on strategies including optimized experimental design, the development of next-generation liquid cells, and the integration of artificial intelligence technologies. First, refining experimental protocols to better replicate realistic sample environments is essential. This may involve, for example, introducing radical scavengers to suppress beam-induced radiolysis byproducts, or employing advanced techniques such as 4D-STEM to improve environmental fidelity. In terms of liquid cell design, further development of graphene-based liquid cells is particularly promising. Enhancing their mechanical stability and reducing fabrication complexity would allow broader application of their atomically thin architecture, thereby improving spatial resolution in LP-TEM. Additionally, next-generation liquid cells should incorporate multiphysics control functionalities—such as tunable electric, thermal, and optical fields—to enable precise environmental regulation. Finally, the incorporation of machine learning and deep learning techniques into LP-TEM imaging represents a powerful direction. Deep learning has already shown remarkable success in image denoising, offering a pathway to significantly enhance image resolution in electron beam-sensitive systems. Furthermore, the interpretive capabilities of deep neural networks can be leveraged to track the dynamics of large populations of particles in TEM image sequences, enabling higher-level analysis of particle behavior and uncovering mechanistic insights that are difficult to access through conventional approaches. For example, statistical information and the high-volume temporal data of nanomaterials generated by TEM often contains important underlying insights that are difficult to extract manually. AI

techniques can analyze such statistical information and reveal those underlying mechanisms. The Transformer architecture has a strong ability to process temporal information. It is well suited for the analysis of time-sequential TEM images. Future studies can improve and train models based on the Transformer architecture to better adapt to time-resolved TEM studies. In addition, specific dynamic behaviors of nanomaterials are difficult to describe by physical equations, whereas AI such as VAE (Variational Autoencoder) can reconstruct these behaviors through black-box modeling. Overall, AI techniques show great promise for broad applications in LP-TEM studies of nanomaterials.

Data Availability Statement

Data will be made available on request.

Funding

This work was supported by the Research Start-up Fund for New Teachers of Southeast University under Grant 4006012510.

Conflicts of Interest

Qiubo Zhang serves as a Editorial Board Member of the *Journal of Advanced Materials Research*. To ensure the integrity of the peer-review process, Qiubo Zhang had no involvement in the editorial handling, peer review, or decision-making process for this manuscript. The manuscript was handled independently by another editor in accordance with the journal's editorial policies. The remaining authors declare no conflicts of interest. Note: The SEU-FEI Nano-Pico Center is a joint laboratory between Southeast University and FEI Company (Thermo Fisher Scientific). The authors confirm that this affiliation did not influence the objectivity of this review.

AI Use Statement

The authors declare that ChatGPT-5 was used solely for language polishing in the preparation of this manuscript, and the authors have reviewed and take full responsibility for the content.

Ethical Approval and Consent to Participate

Not applicable.

References

[1] Zhou, Z. Y., Tian, N., Li, J. T., Broadwell, I., & Sun, S. G. (2011). Nanomaterials of high surface energy with exceptional properties in catalysis and energy storage. *Chemical Society Reviews, 40*(7), 4167-4185. [CrossRef]

[2] Yang, X., Yang, M., Pang, B., Vara, M., & Xia, Y. (2015). Gold nanomaterials at work in biomedicine. *Chemical reviews, 115*(19), 10410-10488. [CrossRef]

[3] Franklin, A. D. (2015). Nanomaterials in transistors: From high-performance to thin-film applications. *Science, 349*(6249), aab2750. [CrossRef]

[4] Zheng, H., Smith, R. K., Jun, Y. W., Kisielowski, C., Dahmen, U., & Alivisatos, A. P. (2009). Observation of single colloidal platinum nanocrystal growth trajectories. *Science, 324*(5932), 1309-1312. [CrossRef]

[5] Yuk, J. M., Park, J., Ercius, P., Kim, K., Hellebusch, D. J., Crommie, M. F., ... & Alivisatos, A. P. (2012). High-resolution EM of colloidal nanocrystal growth using graphene liquid cells. *Science, 336*(6077), 61-64. [CrossRef]

[6] LaMer, V. K., & Dinegar, R. H. (1950). Theory, production and mechanism of formation of monodispersed hydrosols. *Journal of the american chemical society, 72*(11), 4847-4854. [CrossRef]

[7] Di Vece, M., Grandjean, D., Van Bael, M. J., Romero, C. P., Wang, X., Decoster, S., ... & Lievens, P. (2008). Hydrogen-induced ostwald ripening at room temperature in a Pd nanocluster film. *Physical review letters, 100*(23), 236105. [CrossRef]

[8] Li, D., Nielsen, M. H., Lee, J. R., Frandsen, C., Banfield, J. F., & De Yoreo, J. J. (2012). Direction-specific interactions control crystal growth by oriented attachment. *Science, 336*(6084), 1014-1018. [CrossRef]

[9] Xin, H. L., & Zheng, H. (2012). In situ observation of oscillatory growth of bismuth nanoparticles. *Nano letters, 12*(3), 1470-1474. [CrossRef]

[10] Liao, H. G., Zherebetskyy, D., Xin, H., Czarnik, C., Ercius, P., Elmlund, H., ... & Zheng, H. (2014). Facet development during platinum nanocube growth. *Science, 345*(6199), 916-919. [CrossRef]

[11] Loh, N. D., Sen, S., Bosman, M., Tan, S. F., Zhong, J., Nijhuis, C. A., ... & Mirsaidov, U. (2017). Multistep nucleation of nanocrystals in aqueous solution. *Nature chemistry, 9*(1), 77-82. [CrossRef]

[12] Zhang, Q., Peng, X., Nie, Y., Zheng, Q., Shangguan, J., Zhu, C., ... & Zheng, H. (2022). Defect-mediated ripening of core-shell nanostructures. *Nature communications, 13*(1), 2211. [CrossRef]

[13] Liang, W. I., Zhang, X., Bustillo, K., Chiu, C. H., Wu, W. W., Xu, J., ... & Zheng, H. (2015). In situ study of spinel ferrite nanocrystal growth using liquid cell transmission electron microscopy. *Chemistry of Materials, 27*(23), 8146-8152. [CrossRef]

[14] Liao, H. G., Cui, L., Whitelam, S., & Zheng, H. (2012). Real-Time Imaging of Pt_3Fe Nanorod Growth

in Solution. *Science*, *336*(6084), 1011-1014. [CrossRef]

[15] Yang, J., Zeng, Z., Kang, J., Betzler, S., Czarnik, C., Zhang, X., ... & Zheng, H. (2019). Formation of two-dimensional transition metal oxide nanosheets with nanoparticles as intermediates. *Nature materials*, *18*(9), 970-976. [CrossRef]

[16] Ye, H., Wu, C., Cao, D., Zhang, G., Sun, Y., Zhu, Y., ... & Wang, R. (2026). Atomically resolved two-dimensional amorphous nuclei formed during MoS_2 chemical vapor deposition. *Science*, *391*(6728), 622-627. [CrossRef]

[17] Long, R., Zhou, S., Wiley, B. J., & Xiong, Y. (2014). Oxidative etching for controlled synthesis of metal nanocrystals: atomic addition and subtraction. *Chemical Society Reviews*, *43*(17), 6288-6310. [CrossRef]

[18] Hauwiller, M. R., Ondry, J. C., Chan, C. M., Khandekar, P., Yu, J., & Alivisatos, A. P. (2019). Gold nanocrystal etching as a means of probing the dynamic chemical environment in graphene liquid cell electron microscopy. *Journal of the American Chemical Society*, *141*(10), 4428-4437. [CrossRef]

[19] Hutzler, A., Fritsch, B., Jank, M. P., Branscheid, R., Martens, R. C., Spiecker, E., & März, M. (2019). In situ liquid cell TEM studies on etching and growth mechanisms of gold nanoparticles at a solid–liquid–gas interface. *Advanced Materials Interfaces*, *6*(20), 1901027. [CrossRef]

[20] Su, T., Wang, Z. L., & Wang, Z. (2019). In situ observations of shell growth and oxidative etching behaviors of Pd nanoparticles in solutions by liquid cell transmission electron microscopy. *Small*, *15*(14), 1900050. [CrossRef]

[21] Zheng, Q., Shangguan, J., Li, X., Zhang, Q., Bustillo, K. C., Wang, L. W., ... & Zheng, H. (2021). Observation of surface ligands-controlled etching of palladium nanocrystals. *Nano Letters*, *21*(15), 6640-6647. [CrossRef]

[22] Wang, W., Xu, T., Bai, T., Zhu, C., Zhang, Q., Zhang, H., ... & Sun, L. (2020). Controlled oxidative etching of gold nanorods revealed through in-situ liquid cell electron microscopy. *Science China Materials*, *63*(12), 2599-2605. [CrossRef]

[23] Wang, W., Xu, T., Chen, J., Shangguan, J., Dong, H., Ma, H., ... & Sun, L. (2022). Solid–liquid–gas reaction accelerated by gas molecule tunnelling-like effect. *Nature Materials*, *21*(8), 859-863. [CrossRef]

[24] Zhang, Q., Gao, G., Shen, Y., Peng, X., Shangguan, J., Wang, Y., ... & Zheng, H. (2018). Anomalous Shape Evolution of Ag_2O_2 Nanocrystals Modulated by Surface Adsorbates during Electron Beam Etching. *Nano Letters*, *19*(1), 591-597. [CrossRef]

[25] Ye, X., Jones, M. R., Frechette, L. B., Chen, Q., Powers, A. S., Ercius, P., ... & Alivisatos, A. P. (2016). Single-particle mapping of nonequilibrium nanocrystal transformations. *Science*, *354*(6314), 874-877. [CrossRef]

[26] Shan, H., Gao, W., Xiong, Y., Shi, F., Yan, Y., Ma, Y., ... & Wu, J. (2018). Nanoscale kinetics of asymmetrical corrosion in core-shell nanoparticles. *Nature Communications*, *9*(1), 1011. [CrossRef]

[27] Shi, F., Tieu, P., Hu, H., Peng, J., Zhang, W., Li, F., ... & Wu, J. (2024). Direct in-situ imaging of electrochemical corrosion of Pd-Pt core-shell electrocatalysts. *Nature Communications*, *15*(1), 5084. [CrossRef]

[28] Peng, X., Shangguan, J., Zhang, Q., Hauwiller, M., Yu, H., Nie, Y., ... & Zheng, H. (2024). Unveiling corrosion pathways of Sn nanocrystals through high-resolution liquid cell electron microscopy. *Nano Letters*, *24*(4), 1168-1175. [CrossRef]

[29] Wu, J., Gao, W., Yang, H., & Zuo, J. M. (2017). Dissolution kinetics of oxidative etching of cubic and icosahedral platinum nanoparticles revealed by in situ liquid transmission electron microscopy. *ACS nano*, *11*(2), 1696-1703. [CrossRef]

[30] Grochowski, P., & Trylska, J. (2008). Continuum molecular electrostatics, salt effects, and counterion binding—A review of the Poisson–Boltzmann theory and its modifications. *Biopolymers: Original Research on Biomolecules*, *89*(2), 93-113. [CrossRef]

[31] Kilpatrick, J. I., Loh, S. H., & Jarvis, S. P. (2013). Directly probing the effects of ions on hydration forces at interfaces. *Journal of the American Chemical Society*, *135*(7), 2628-2634. [CrossRef]

[32] Luo, B., Smith, J. W., Ou, Z., & Chen, Q. (2017). Quantifying the Self-Assembly Behavior of Anisotropic Nanoparticles Using Liquid Phase Transmission Electron Microscopy. *Accounts of Chemical Research*, *50*(5), 1125-1133. [CrossRef]

[33] Chen, Q., Cho, H., Manthiram, K., Yoshida, M., Ye, X., & Alivisatos, A. P. (2015). Interaction Potentials of Anisotropic Nanocrystals from the Trajectory Sampling of Particle Motion using in Situ Liquid Phase Transmission Electron Microscopy. *ACS Central Science*, *1*(1), 33-39. [CrossRef]

[34] Zhu, C., Liang, S., Song, E., Zhou, Y., Wang, W., Shan, F., ... & Sun, L. (2018). In-situ liquid cell transmission electron microscopy investigation on oriented attachment of gold nanoparticles. *Nature communications*, *9*(1), 421. [CrossRef]

[35] Liu, Y., Lin, X. M., Sun, Y., & Rajh, T. (2013). In situ visualization of self-assembly of charged gold nanoparticles. *Journal of the American Chemical Society*, *135*(10), 3764-3767. [CrossRef]

[36] Powers, A. S., Liao, H. G., Raja, S. N., Bronstein, N. D., Alivisatos, A. P., & Zheng, H. (2017). Tracking nanoparticle diffusion and interaction during self-assembly in a liquid cell. *Nano letters*, *17*(1), 15-20. [CrossRef]

[37] Park, J., Zheng, H., Lee, W. C., Geissler, P. L., Rabani, E., & Alivisatos, A. P. (2012). Direct Observation of Nanoparticle Superlattice Formation by Using Liquid Cell Transmission Electron Microscopy. *ACS Nano*,

6(3), 2078-2085. [CrossRef]

[38] Ou, Z., Wang, Z., Luo, B., Luijten, E., & Chen, Q. (2020). Kinetic pathways of crystallization at the nanoscale. *Nature materials, 19*(4), 450-455. [CrossRef]

[39] Chen, Q., Whitmer, J. K., Jiang, S., Bae, S. C., Luijten, E., & Granick, S. (2011). Supracolloidal reaction kinetics of Janus spheres. *Science, 331*(6014), 199-202. [CrossRef]

[40] Hong, J., Bae, J. H., Jo, H., Park, H. Y., Lee, S., Hong, S. J., ... & Chun, D. W. (2022). Metastable hexagonal close-packed palladium hydride in liquid cell TEM. *Nature, 603*(7902), 631-636. [CrossRef]

[41] Ross, F. M. (2015). Opportunities and challenges in liquid cell electron microscopy. *Science, 350*(6267), aaa9886. [CrossRef]

[42] Clark, N., Kelly, D. J., Zhou, M., Zou, Y. C., Myung, C. W., Hopkinson, D. G., ... & Haigh, S. J. (2022). Tracking single adatoms in liquid in a transmission electron microscope. *Nature, 609*(7929), 942-947. [CrossRef]

[43] Peng, X., Tu, Q., Zhang, Y., Jun, K., Shen, F., Ogunfunmi, T., ... & Scott, M. C. (2023). Unraveling Li growth kinetics in solid electrolytes due to electron beam charging. *Science Advances, 9*(17), eabq3285. [CrossRef]

[44] Huang, J. Y., Zhong, L., Wang, C. M., Sullivan, J. P., Xu, W., Zhang, L. Q., ... & Li, J. (2010). In Situ Observation of the Electrochemical Lithiation of a Single SnO_2 Nanowire Electrode. *Science*, *330*(6010), 1515-1520. [CrossRef]

[45] Zhong, L., Liu, Y., Han, W. Q., Huang, J. Y., & Mao, S. X. (2017). In Situ Observation of Single-Phase Lithium Intercalation in Sub-25-nm Nanoparticles. *Advanced Materials, 29*(26), 1700236. [CrossRef]

[46] Williamson, M. J., Tromp, R. M., Vereecken, P. M., Hull, R., & Ross, I. F. (2003). Dynamic microscopy of nanoscale cluster growth at the solid–liquid interface. *Nature materials, 2*(8), 532-536. [CrossRef]

[47] Xia, W., Zhang, Q., Xu, F., Ma, H., Chen, J., Qasim, K., ... & Sun, L. (2016). Visualizing the electrochemical lithiation/delithiation behaviors of black phosphorus by in situ transmission electron microscopy. *The Journal of Physical Chemistry C, 120*(11), 5861-5868. [CrossRef]

[48] Zeng, Z., Liang, W. I., Liao, H. G., Xin, H. L., Chu, Y. H., & Zheng, H. (2014). Visualization of Electrode–Electrolyte Interfaces in $LiPF_6$/EC/DEC Electrolyte for Lithium Ion Batteries via in Situ TEM. *Nano Letters*, *14*(4), 1745-1750. [CrossRef]

[49] Leenheer, A. J., Jungjohann, K. L., Zavadil, K. R., Sullivan, J. P., & Harris, C. T. (2015). Lithium Electrodeposition Dynamics in Aprotic Electrolyte Observed in Situ via Transmission Electron Microscopy. *ACS Nano*, *9*(4), 4379-4389. [CrossRef]

[50] Sacci, R. L., Black, J. M., Balke, N., Dudney, N. J., More, K. L., & Unocic, R. R. (2015). Nanoscale imaging of fundamental Li battery chemistry: solid-electrolyte interphase formation and preferential growth of lithium metal nanoclusters. *Nano letters, 15*(3), 2011-2018. [CrossRef]

[51] Dachraoui, W., Pauer, R., Battaglia, C., & Erni, R. (2023). Operando electrochemical liquid cell scanning transmission electron microscopy investigation of the growth and evolution of the mosaic solid electrolyte interphase for lithium-ion batteries. *ACS nano, 17*(20), 20434-20444. [CrossRef]

[52] Li, Y., Li, Y., Pei, A., Yan, K., Sun, Y., Wu, C. L., ... & Cui, Y. (2017). Atomic structure of sensitive battery materials and interfaces revealed by cryo–electron microscopy. *Science, 358*(6362), 506-510. [CrossRef]

[53] Wang, X., Zhang, M., Alvarado, J., Wang, S., Sina, M., Lu, B., ... & Meng, Y. S. (2017). New insights on the structure of electrochemically deposited lithium metal and its solid electrolyte interphases via cryogenic TEM. *Nano letters, 17*(12), 7606-7612. [CrossRef]

[54] Fang, C., Li, J., Zhang, M., Zhang, Y., Yang, F., Lee, J. Z., ... & Meng, Y. S. (2019). Quantifying inactive lithium in lithium metal batteries. *Nature, 572*(7770), 511-515. [CrossRef]

[55] Yang, Y., Louisia, S., Yu, S., Jin, J., Roh, I., Chen, C., ... & Yang, P. (2023). Operando studies reveal active Cu nanograins for CO_2 electroreduction. *Nature, 614*(7971), 262-269. [CrossRef]

[56] Ortiz Pena, N., Ihiawakrim, D., Han, M., Lassalle-Kaiser, B., Carenco, S., Sanchez, C., ... & Ersen, O. (2019). Morphological and Structural Evolution of Co_3O_4 Nanoparticles Revealed by in Situ Electrochemical Transmission Electron Microscopy during Electrocatalytic Water Oxidation. *ACS Nano*, *13*(10), 11372-11381. [CrossRef]

[57] Kim, J., Park, A., Kim, J., Kwak, S. J., Lee, J. Y., Lee, D., ... & Park, J. (2022). Observation of H_2 Evolution and Electrolyte Diffusion on MoS_2 Monolayer by In Situ Liquid Phase Transmission Electron Microscopy. *Advanced Materials*, *34*(47), 2206066. [CrossRef]

[58] Zhang, Q., Song, Z., Sun, X., Liu, Y., Wan, J., Betzler, S. B., ... & Zheng, H. (2024). Atomic dynamics of electrified solid–liquid interfaces in liquid-cell TEM. *Nature, 630*(8017), 643-647. [CrossRef]

Ziming Shang is currently pursuing the PhD. degree at the School of Integrated Circuits, Southeast University, Nanjing 210096, CN. His research interests include AI-assisted electron microscopy image processing and the synthesis of high-entropy alloy materials. (Email: ziming_shang@seu.edu.cn)

Yu Su is currently pursuing the PhD. degree at the School of Integrated Circuits, Southeast University, Nanjing 210096, CN. His research interests include in Situ characterization by transmission electron microscopy, the growth of two-dimensional semiconductor materials, and device fabrication. (Email: icsuyu@seu.edu.cn)

Yi Chen is currently pursuing the Ph.D. degree at University of California, Berkeley 94720, USA. (Email: ychen10@lbl.gov)

Qiubo Zhang is a Distinguished Young Professor and PhD supervisor at the School of Integrated Circuits, Southeast University, Nanjing 210096, China, and a recipient of a national high-level talent program. His research focuses on in situ transmission electron microscopy studies of electronic materials and devices under external-field loading conditions, with emphasis on nanoscale structure–property relationships. He has published more than 50 SCI-indexed papers in leading international journals, including Nature, Nature Materials, Nature Nanotechnology, Nature Communications, and Science Advances, and has applied for two U.S. invention patents. He serves as a Young Editorial Board Member of Nano-Micro Letters and Rare Metals, and as an Associate Editor of Advanced Materials Research. (Email: qiubozhang@seu.edu.cn)